Australian Journal of Basic and Applied Sciences, 7(7): 348-357, 2013
ISSN 1991-8178

Implementation of Anti-Windup PI Speed Controller for Induction Motor Drive Using dSPACE and Matlab/Simulink Environment

[1]M.H.N. Talib, [2]Z.Ibrahim, [3]N. Abdul Rahim, [4]A.S.A. Hasim

[1,2] Faculty of Electrical Engineering, Universiti Teknikal Malaysia Melaka
[3]UMPEDAC, Universiti Malaya,
[4]Faculty of Engineering, Universiti Pertahanan Nasional Malaysia,
[1,2] Melaka, Malaysia.
[3,4] Kuala Lumpur, Malaysia

Abstract: This paper presents the design, analysis and implementation of speed control drive indirect Field Oriented Control (FOC) induction motor using a dSPACE DS1103 digital-signal-processor-based real-time data acquisition control system and MATLAB/Simulink environment. The details design of speed control indirect Field Oriented Control (FOC) induction motor drive with Anti-Windup PI controllers' (AWPI) is discussed. In addition, the controller designed is focused on the mathematical determination of proportional integral (PI) controller which is usually obtained by trial and error approached. Three PI controllers are used in speed and current loops to control the Space Vector Pulse Width Modulation Technique (SVPWM) in FOC scheme. Simulation and experimental test results at rated voltage, speed and load disturbance are verified the effectiveness of the design approached.

Key words: PI controller; Anti-Windup; Induction Motor Drive; Field Oriented Control (FOC), Space Vector Pulse Width Modulation (SVPWM)

INTRODUCTION

Simple structure, ruggedness, high reliability, low cost and minimum maintenance are the main criteria offered by induction motor. With the self advantages over its structure, the advancement of the control methods makes induction motor drives the most popular choices in industries (Vas.P, 1998, B.K.Bose, 2002). The control method of induction motor drive can be classified into two categories known as scalar control and vector control. Scalar control or constant volt/freq ratio offers simple structure to maintain the constant flux in the machines. However, the torque and flux dynamic performance is extremely poor.

The demands of high performance motor drive which have good transient and steady state performances introduce the vector control category. The vector control not only control the voltage amplitude and frequency as scalar control methods, but also the instantaneous position of the voltage, current and flux vectors. The basic principle of the FOC method is to independently control the flux and torque component in similar fashion as separately excited DC machine. This improves significantly the dynamic behavior of the drive. In this method the instantaneous stator current are transformed into a coordinate system that rotates in synchronism to align with the rotor, stator or air gap flux vector. The FOC method guarantees flux and torque decoupling. The first field oriented control (FOC) methods were formulated in early of 70s by K. Hasse (Indirect FOC) and F. Blaschke (Direct FOC)(De Doncker *et al*., 1995, Casadei *et al*., 2002, Santisteban and Stephan, 2001). Direct FOC method used hall sensor mounted in the air gap to measure the flux magnitude and flux angle for field orientation. Meanwhile, the indirect FOC method used estimation or calculation of a slip frequency derived from the rotor dynamic equation to achieve flux orientation. Thus, indirect FOC offers easier implementation and cost effectiveness compared to the direct FOC method. However, this method needs accurate knowledge of rotor time constant. The rotor time constant will change during motor operation due to temperature and flux changes. Many researches focused on solving this issue such as parameters sensitivity and adaption(Krishnan and Bharadwaj, 1991)

There are several types of vector control scheme such as PI control, fuzzy PI control, Artificial Intelligent control, variable structure control and many more used to get the best performance of the motor as well as to withstand the load external disturbances, unpredictable parameter variations, and nonlinear plant(Eun-Chul *et al*., 2003, Gaolin *et al*., 2008, Kuo-Kai and Hsin-Jang, 1995, Sousa *et al*., 1995, Ba-Razzouk *et al*., 1997). Among these techniques, PI controller is one of the simple and practical speed control methods. This technique is able to independently control the torque and the flux-producing component of the stator current in a speed range. Unfortunately, these gains are usually tuned on a trial and error basis. The performance of the motor are really relied on the gain of the individual PI controllers.

Conventional or linear PI controller does not have output magnitude limiters, could cause damage to the real system due to relatively large output value. Introducing integrator limiter and saturation limiter provide

Corresponding Author: M.H.N. Talib, Faculty of Electrical Engineering, Universiti Teknikal Malaysia Melaka
E-mail: hairulnizam@utem.edu.my

some protection to the system. However, this saturation limiter cause accumulating error, thus producing large overshoot, slow settling time and sometimes instability to the system(Bohn and Atherton, 1995, Hwi-Beon, 1998, Scottedward Hodel and Hall, 2001, Espina *et al*., 2009, Jong-Woo and Sang-Cheol, 2009). Several Anti-windup PI controllers were introduced to solve this wind up phenomenon such as AWPI with dead zone, AWPI condition, AWPI with tracking and also other some improvement technique. All the AWPI controller technique is able to solve the wind up problem. However, all the schemes have their own advantages and disadvantages. Thus, the AWPI condition is used in this paper due to its simple, good performance and robustness.

This paper focused on the implementation of indirect FOC method based on SVPWM technique by using Dspace DSP DS1103. Details design of FOC, IM model and PI controller are presented. The PI controller design is adopted based on the second order system design which has more simple technique and direct mathematical formulation in comparison to the classical gain tuning method or symmetric optimum criterion(Eun-Chul *et al*., 2003, Foo *et al*., 2009, Zelechowski *et al*., 2005, Espina *et al*., 2009). All the simulation and experimental test are conducted by using rated voltage supply, rated speed and rated load disturbance. Finally the simulation and real time experimental results of the motor performance are analyzed.

Induction Motor Drive:

Three phase induction motor drive can be divided into a few main parts which is discussed in this section include induction motor model, FOC method, SVPWM, PI controllers and transformation.

A. Three Phase Induction Motor Model:

By applying space vector transformation to a three-phase system, the dynamic behavior of induction motor can be represented in mathematical equations as in (1)-(4) in synchronous rotating frame(Casadei *et al*., 2002, Vas.P, 1998, B.K.Bose, 2002).

Stator voltage equations:

$$\begin{aligned}\bar{V}_{sd} &= R_s\bar{I}_{sd} + \frac{d\bar{\varphi}_{sd}}{dt} - \omega_s\bar{\varphi}_{sq}\\ \bar{V}_{sq} &= R_s\bar{I}_{sq} + \frac{d\bar{\varphi}_{sq}}{dt} + \omega_s\bar{\varphi}_{sd}\end{aligned} \quad (1)$$

Rotor Voltage equations:

$$\begin{aligned}\bar{V}_{rd} = 0 &= R_r\bar{I}_{rd} + \frac{d\bar{\varphi}_{rd}}{dt} - (\omega_s - \omega_r)\bar{\varphi}_{rq}\\ \bar{V}_{rq} = 0 &= R_r\bar{I}_{rq} + \frac{d\bar{\varphi}_{rq}}{dt} + (\omega_s - \omega_r)\bar{\varphi}_{rd}\end{aligned} \quad (2)$$

Stator Flux equations:

$$\begin{aligned}\bar{\varphi}_{sd} &= L_s\bar{I}_{sd} + L_m\bar{I}_{rd}\\ \bar{\varphi}_{sq} &= L_s\bar{I}_{sq} + L_m\bar{I}_{rq}\end{aligned} \quad (3)$$

Rotor Flux equations:

$$\begin{aligned}\bar{\varphi}_{rd} &= L_m\bar{I}_{sd} + L_r\bar{I}_{rd}\\ \bar{\varphi}_{rq} &= L_m\bar{I}_{sq} + L_r\bar{I}_{rq}\end{aligned} \quad (4)$$

where $\bar{V}$, $\bar{I}$, $\bar{\varphi}$, are the voltages, current and flux. Meanwhile subscript d, q represent the dq axis; s and r represent stator and rotor component. The stator and rotor resistance and inductance are denoted as *Rs*, *Rr* and *Ls*, *Lr* , whereas *Lm* is the mutual inductance. ω_s and ω_r represent the synchronous speed and mechanical speed respectively.

The electromagnetic torque, T_e developed by the IM can be expressed in the terms of flux and current space vector in the mechanical torque equation (5);

$$\begin{aligned}T_e &= \frac{3}{2}\frac{P}{2}\left(\bar{\varphi}_{ds}\bar{I}_{sq} - \bar{\varphi}_{qs}\bar{I}_{sd}\right)\\ T_e - T_L &= J\frac{d\omega_r}{dt} + B\omega_r\end{aligned} \quad (5)$$

where P, T_L, J and B denote respectively the number of poles, external load, inertia and friction of the IM coupled with the permanent magnet dc-machine respectively.

B. FOC Block Diagram:

The FOC imitates the concept of separately excited dc motor drive where the torque and the flux are controlled by two independent orthogonal variables known as the armature and field currents. **Error! Reference source not found.**shows the block diagram of indirect FOC scheme.

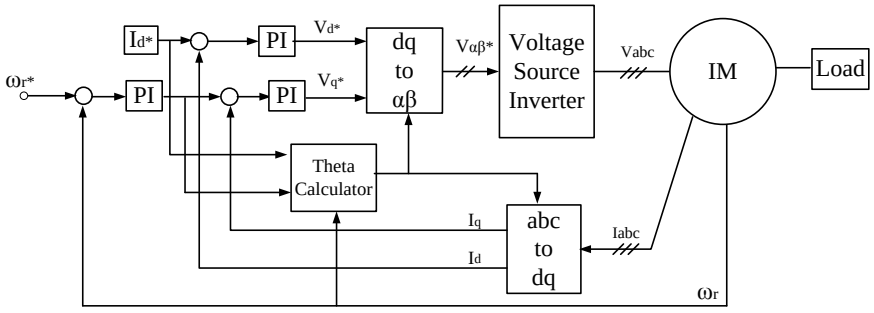

Fig. 1: Two induction motor drive in FLI system diagram

In this system, the rotating coordinate reference frame having direct axis is aligned with the rotor flux vector that rotate at the stator frequency. Therefore, the q-component of the rotor flux is null and the expression of the electromagnetic torque becomes:

$$T_e = \frac{3}{2}\frac{P}{2}\frac{L_m^2}{L_r}\bar{I}_{sd}\bar{I}_{sq} \tag{6}$$

Based on the rotor voltage direct axis equation of induction motor, the rotor flux linkage can be estimated using this formula;

$$\hat{\psi}_r = \frac{L_m I_{sd}}{1+\tau_r s} \tag{7}$$

where, τ_r is the rotor time constant.

The slip frequency ω_{sl} is obtained from the rotor voltage quadrature axis equation by:

$$\omega_{sl} = \frac{L_m R_r I_{sq}}{\hat{\psi}_r L_r} \tag{8}$$

The rotor flux position, θ_e for coordinate transform is generated from the integration of rotor speed, ω_r and slip frequency, ω_{sl}.

$$\theta_e = \int \omega_r + \omega_{sl} \tag{9}$$

The reference torque current, *Iq** is generated from the error of speed demand, ωr* and actual measure speed, ωr with the speed PI controller. Then the *Iq** is compared with the actual torque current component, *Iq* and this gives the torque current error. This error is processed to generate the reference voltage torque component, *Vq**. On the other hand, the reference flux component current, *Id** which has been set earlier to a constant value is compared with the actual values of this variable, *Id*. The error signal is applied to PI controller to generate the command values of flux voltage components, *Vd**. These reference voltages are then transformed into stationary reference frame voltage by dq to αβ transformation for SVPWM modulation process. The transformation between stationary a-b-c frame, stationary α-β frame and synchronously rotating d-q frame are described as the following equation (10) to (12).

- Clarke; convert stationary a-b-c frame to stationary α-β

$$\begin{matrix} I_\alpha \\ I_\beta \end{matrix} = \begin{bmatrix} \frac{2}{3} & -\frac{1}{3} & -\frac{1}{3} \\ 0 & \frac{1}{\sqrt{3}} & -\frac{1}{\sqrt{3}} \end{bmatrix} \begin{matrix} I_a \\ I_b \\ I_c \end{matrix} \tag{10}$$

- Park; convert stationary α-β frame to rotating d-q frame.

$$\begin{matrix} I_d \\ I_q \end{matrix} = \begin{bmatrix} \cos\theta & \sin\theta \\ -\sin\theta & \cos\theta \end{bmatrix} \begin{matrix} I_\alpha \\ I_\beta \end{matrix} \tag{11}$$

- Inverse Park; convert rotating d-q frame to stationary α-β frame.

$$\begin{matrix} I_\alpha \\ I_\beta \end{matrix} = \begin{bmatrix} \cos\theta & -\sin\theta \\ \sin\theta & \cos\theta \end{bmatrix} \begin{matrix} I_d \\ I_q \end{matrix} \quad (12)$$

C. Space Vector Pulse Width Modulation (SVPWM):

The major purpose of the SVPWM is to generate a variable voltage variable frequency three phase supply to the AC drive application. In the FOC algorithm, the control variables are expressed in rotating frame. The current vector of Iq and Id are transform to voltage vector after current regulation mechanism and the inverse Park transform. The SVPWM operate in a complex plane divided in the six active sectors and two zero vectors as shown in **Error! Reference source not found.**The eight switching state vector are defined by combination of on/off of the upper and lower switches in the inverter power circuit. If a constant reference voltage vector V* is given in one sampling period, the vector can be generated using two adjacent active vectors, V1 and V2 and zero vector (V0 and V7). Meanwhile T_1 and T_2 are referred to the effective time corresponding to V1 and V2 respectively. For the remaining time, $T_0=T_S-T_1-T_2$ is corresponding to the zero vector, where T_S is the sampling period. These two active vectors are considered as the effective vector to generate desire output voltage.

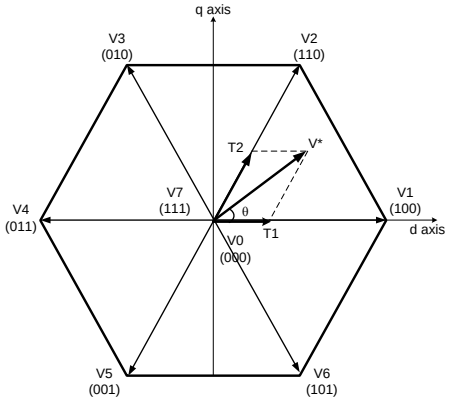

Fig. 2: Space Vector diagram

D. PI Controller Design

As refer to the vector block diagram in Figure 1, three PI controllers are used for the torque current component, flux current component and speed. Based on the motor equation 1, in stationary reference frame the block diagram of torque and flux component loop can be simplified as 0

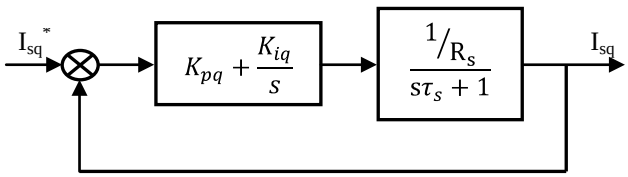

Fig. 3: Simplified torque component current loop control

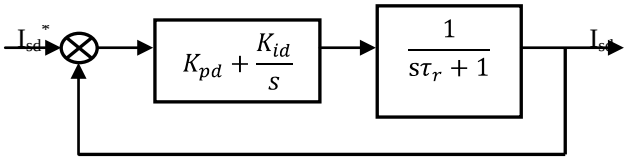

Fig. 4: Simplified flux component current loop control

The closed loops for torque and flux component above are shown in equation (13) and (14)

$$\frac{I_{sq}^{*}}{I_{sq}} = \frac{\left(K_{pq} + \frac{K_{iq}}{s}\right)\left(\frac{1/R_s}{s\tau_s + 1}\right)}{1 + \left(K_{pq} + \frac{K_{iq}}{s}\right)\left(\frac{1/R_s}{s\tau_s + 1}\right)} \quad (13)$$

$$\frac{I_{sd}^{*}}{I_{sd}} = \frac{\left(K_{pd} + \frac{K_{id}}{s}\right)\left(\frac{1}{s\tau_r + 1}\right)}{1 + \left(K_{pd} + \frac{K_{id}}{s}\right)\left(\frac{1}{s\tau_r + 1}\right)} \quad (14)$$

Where $\tau_s = \frac{L_s}{R_s}$ and $\tau_r = \frac{L_r}{R_r}$ is the stator and rotor time constant respectively. The speed loop block diagram is illustrated in 0based on the mechanical motor equation.

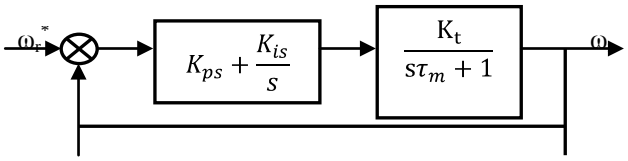

Fig. 5: Simplified speed loop control

Where $\tau_m = \frac{J}{B}$ a is the motor mechanical time constant and torque constant, Kt is given as:

$$K_t = \frac{3}{2}\frac{P}{2}\frac{L_m^2}{L_s}\bar{I}_{sd} \quad (15)$$

The speed closed loop transfer function, is given as below:

$$\frac{\omega_r^{*}}{\omega_r} = \frac{\left(K_{ps} + \frac{K_{is}}{s}\right)\left(\frac{K_t}{s\tau_m + 1}\right)}{1 + \left(K_{ps} + \frac{K_{is}}{s}\right)\left(\frac{K_t}{s\tau_m + 1}\right)} \quad (16)$$

The denominator of the general second order system governed by;

$$s^2 + 2\varsigma\omega_n + \omega_n^2 \quad (17)$$

Where ω_n is the natural frequency of the closed-loop system and ς is the damping ratio.

By comparing the denominator of the closed loop transfer function with equation (17), the value of Kp and Ki can be determined. The gain of the PI controller are shown in 0The values are obtain based on the calculation above with ς is set at 1 and ω_n is set at 100Hz, 10Hz and 1Hz for torque loop, flux loop and speed loop respectively.

Table 1: Pi Controller Parameters

PI Controller	Value
Speed Controller	Kp=0.135 Ki=0.4256
Flux Controller	Kp=10.3 Ki=355
Torque Controller	Kp=30.3 Ki=10607

The main objective of the AW scheme is to avoid the saturation in integrator which causes high overshoot and long settling time. Large step change or large external load disturbance applied causes the PI controller to saturate. This windup phenomenon results in inconsistency between the real plant input and the controller output. In order to overcome the wind up problem, the integral state is separately controlled depending on whether the PI controller output is saturated or not based on the anti-windup structure in Figure 6.

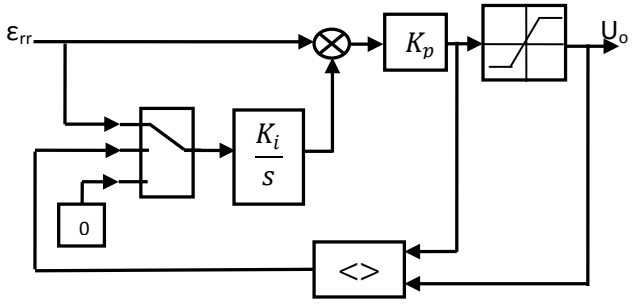

Fig. 6: AWPI conditioned

Simulation and Experiment setup:

Simulation has been done by using Simulink/Matlab Tools to verify the FOC scheme and the controller design. A dedicated speed range and torque load is applied to understand the performances of the FOC. The details of three-phase induction motor parameters are shown in Appendix 1.

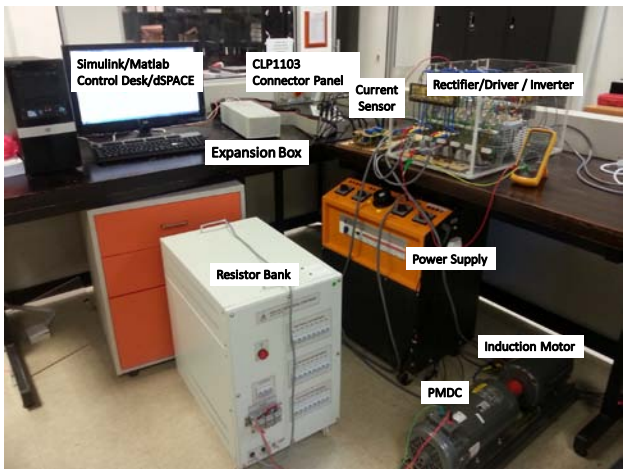

Fig. 7: The experimental setup

The experimental setup consists of software and hardware components. It can be divided into three main parts as power components, controller part and transducer part as shown in **Error! Reference source not found.**The power components consist of three phase power supply, three phase rectifier module (SEMiX341D16s), DC link capacitor (2200µF, 450VDC), inverter (semikron SEMiX252GB126HDs IGBT modul), 1.5kW Baldor induction motor, 2.2kW Baldor Permanent magnet DC motor. The DC link voltage for the voltage source inverter is achieved through three-phase diode bridge rectifier module. The permanent magnet DC machine is used as the load of the induction motor.

The controller part consists of software and hardware components such as dSPACE DS1103 Workstation, Simulink/Matlab, Expansion Box with TMS320F240 DSP, CPL1103 Connector panel, optocoupler circuit (HCPL-3120) and gate drive circuit (SKYPER 32Pro R). The FOC block diagram was modeled using MATLAB/Simulink with dSPACE block sets. The SVPWM generated signal is connected to the DSP1103 bit out module from Real Time Interface (RTI) libraries. The dSPACE 1103 DSP card was used to carry out the real time algorithm. Then, the C code is generated by Real Time Workshop (RTW) to produce switching signals. These switching signals trigger the gate drive to control the three phase inverter which is connected to digital input output (I/O) of CLP1103 connector panel. The opto-coupler is used as protection device to interface the switching signals from DSP controller board to the IGBT modules. Thus, the inverter provides required voltage to control the motor operation.

The transducer part consist of Hall-effect current sensor circuit (LEM HY-10P) and incremental optical encoder (E3-500-500-IE-H-T-B) which has 500 pulses per revolution. The actual stator motor currents are measured by using the current sensor connected to ADC BNC connecter at CLP1103 connector panel. Then, the signals are process through the ADC converter block to provide the current feedback to the system. The speed of the motor is measured by an optical incremental encoder, which is mounted at the rotor-shaft end. It is then fed to the encoder 1 (Inc 1) in the CLP1103 connector panel. The signals are process through encoder set position module to calculate the motor speed for the feedback. The related input and output data can be monitored and controlled by using the Control Desk in real-time on the workstation.

RESULTS AND DISCUSSION

The simulation and experimental test is conducted based on the block diagram in 0 The IM drive system was tested under no load and loaded conditions to verify the system design. The voltage supply is set at rated voltage 380 Vrms and the switching frequency is set at 8kHz. For the experimental test, the sampling time is set at 50µs. Similar value of PI controllers and motor parameters are used in the simulation and experimentation test.

E. Operation Under No-Load Condition:

For the no load condition, the motor is test to operate at standstill, rated forward direction and rated reverse direction. 0shows the simulation and experimentation speed performance at zero speed, then 1400rpm in forward and reverse operation.

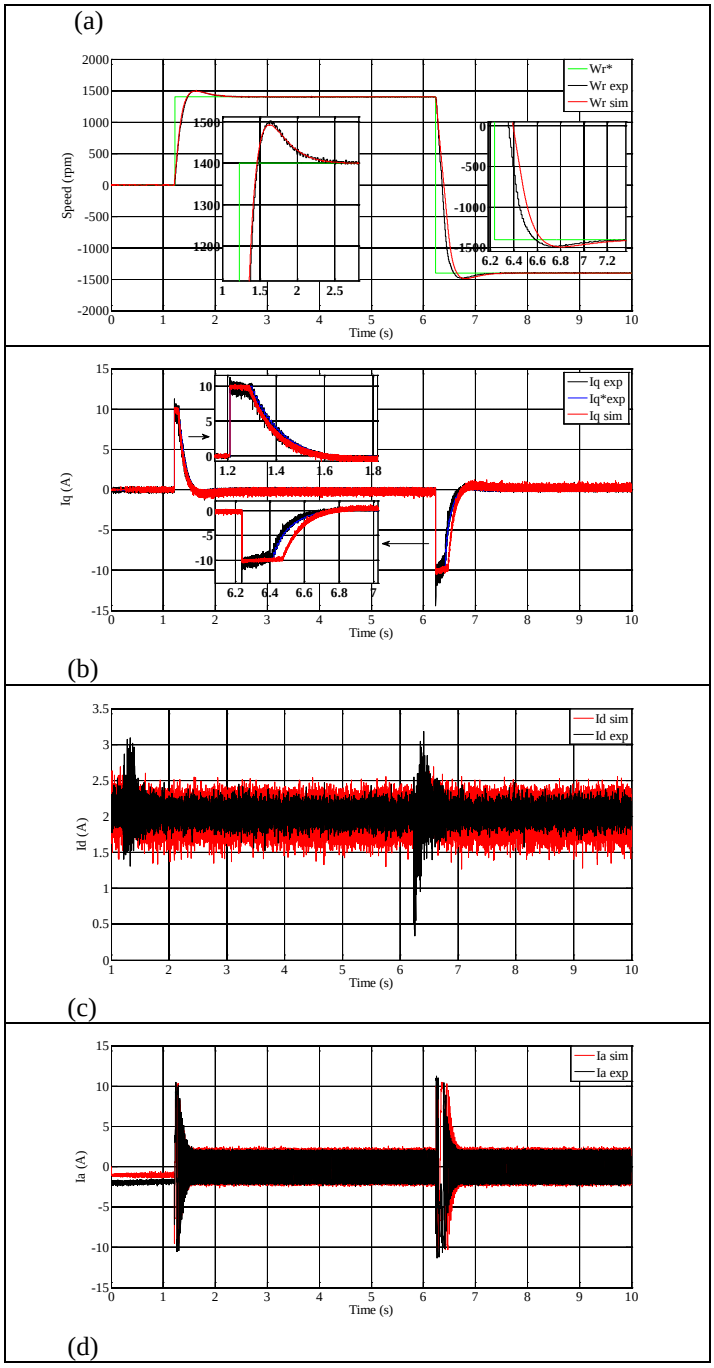

Fig. 8: Simulation and experiment resulta during during standstill, forward and reverse operation, (a) Speed response (b) Torque current response (d) Flux current response and (d) Phase 'a' Current response.

Based on Figure 8(a), good tracking performance is achieved with small percentage of overshoot, 7% during forward and reverse operations. From the torque characteristics in Figure 8(b), the higher torque responses during speed demand changes are noticed. The torque is limited to 10A. Higher overshoot during speed changed demand especially during forward to reverse operation with 14.4Nm maximum value for experiment result. Higher transient electrical torque produces faster speed response during this condition. Based on the current responses, the higher currents occurred during start up condition, during speed reversal and when external loads are applied. From the torque response, higher load condition experience higher stator current and vice versa. This is in line with the motor operation principle. The average peak current during steady state condition is about 2A and 2.2A for experiment and simulation respectively. Lower current during real test is due to the low pass filter effect at the current sensor circuit.

F. Load Rejection:

The load rejection capabilities of the design were investigated. For simulation, 8.5Nm torque was applied in such a way to observe the drives under load rejection properties. Meanwhile in experiment, the load disturbance operation was accomplished through the DC machine using the load bank switches. The permanent magnet DC machine operates as a generator by connecting the armature terminals to the resistor bank. The external resistor of the DC machines is set to produce rated current load at IM. Based on the result in **Error! Reference source not found.**(a), the speed is reduced to 1144rpm for simulation and 1158rpm for experiment before it can be recovered within 1s when rated is applied to the motor. The q-axis stator current increase significantly when the full load is applied as shown in Figure 9(b).

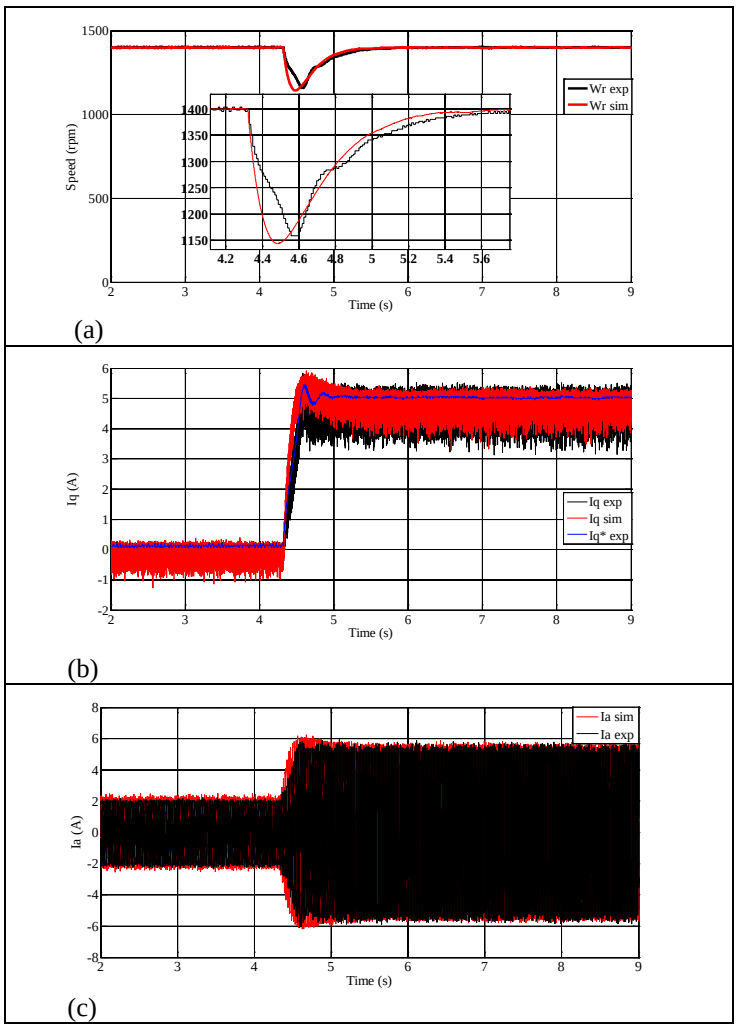

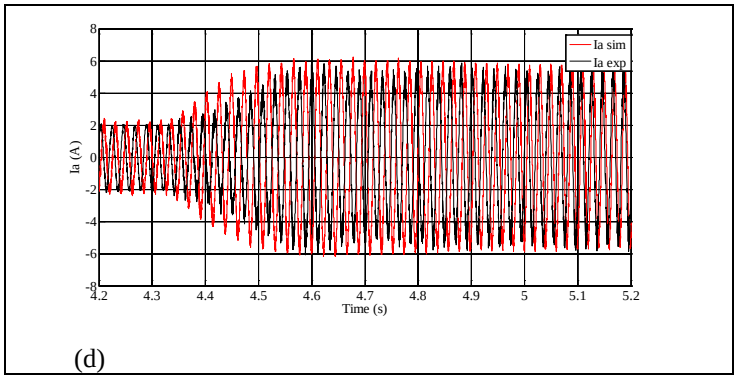

Fig. 9: Simulation and experiment result during load dirstubunce, (a) Speed response and (b) Torque current response (c) Phase 'a' Current response (d) Zoom of Phase Current response during load disturbance

Figure 9 (c) and (d) depict phase A stator current before and after the load disturbance is applied. It may be observed that the stator phase 'a' current reference is significantly increased as the load applied is increased. Further investigation on the result shows the amplitude of the phase current increase from 2.0 to 5.61A for experiment and 2.2A to 5.83A for simulation result. Slide phase shift is noticed due to transient response effect between simulation and experimental results.

Conclusion:

This paper presents the detailed design of indirect FOC method with calculative PI design procedure. All the simulation and experimental tests were carried out at rated voltage, speed and load disturbance. The behavior of the motor performance shows the independent control of torque and flux components principle in FOC is achieved. The results show very significant relation between Matlab/Simulink simulation and dSPACE system with DS1103 controller board experiment results. The calculative based PI controller design is able to work effectively on simulation and experimentation.

ACKNOWLEDGEMENT

The authors would like to acknowledge their gratitude to Faculty of Electrical Engineering Universiti Teknikal Malaysia Melaka for providing the resources and support in this study.

Appendix:

Appendix1: Induction motor parameters

Motor Specifications	Value
Rated Voltage	380 V
Rated Frequency	50 Hz
Poles	4
Rated Speed	1430 rpm
Stator Resistance	3.45 Ω
Rotor Resistance	3.6141 Ω
Stator Inductance	0.3246 H
Rotor Inductance	0.3252 H
Magnetizing Inductance	0.3117 H
Inertia	0.02kgm^2
Viscous Friction	0.001 Nm/(rad/s)

REFERENCES

Bose, B.K., 2002. *Modern Power Electronic and AC Motor Drive*, Prentice Hall PTR.

Ba-Razzouk, A., A. Cheriti, G. Olivier, & P. Sicard, 1997. Field-oriented control of induction motors using neural-network decouplers. *Power Electronics, IEEE Transactions on*, 12: 752-763.

Bohn, C. & D.P. Atherton, 1995. An analysis package comparing PID anti-windup strategies. *Control Systems, IEEE*, 15: 34-40.

Casadei, D., F. Profumo, G. Serra, & A. Tani, 2002. FOC and DTC: two viable schemes for induction motors torque control. *Power Electronics, IEEE Transactions on*, 17: 779-787.

De Doncker, R.W., F. Profumo, M. Pastorelli, & P. Ferraris, 1995. Comparison of universal field oriented (UFO) controllers in different reference frames. *Power Electronics, IEEE Transactions on,* 10: 205-213.

Espina, J., A. Arias, J. Balcells, & C. Ortega, 2009. Year. Speed anti-windup PI strategies review for field oriented control of permanent magnet synchronous machines. *In:* Compatibility and Power Electronics, CPE'09., 2009. IEEE, 279-285.

Eun-Chul, S., P. Tae-Sik, O. Won-Hyun, & Y. Ji-Yoon, 2003. Year. A design method of PI controller for an induction motor with parameter variation. *In:* Industrial Electronics Society, 2003. IECON '03. The 29th Annual Conference of the IEEE, 2-6: 408-413.

Foo, G., C.S. Goon, & M.F. Rahman, 2009. Year. Analysis and design of the SVM direct torque and flux control scheme for IPM synchronous motors. *In:* Electrical Machines and Systems, 2009. ICEMS 2009. International Conference on, pp: 1-6.

Gaolin, W., Y. Yong, Y. Rongfeng, C. Wei, & X. Dianguo, 2008. Year. A robust speed controller for speed sensorless field-oriented controlled induction motor drives. *In:* Vehicle Power and Propulsion Conference, 2008. VPPC '08. IEEE, 3-5: 1-4.

Hwi-Beon, S., 1998. New antiwindup PI controller for variable-speed motor drives. *Industrial Electronics, IEEE Transactions on,* 45: 445-450.

Jong-Woo, C. & L. Sang-Cheol, 2009. Antiwindup Strategy for PI-Type Speed Controller. *Industrial Electronics, IEEE Transactions on,* 56: 2039-2046.

Krishnan, R. & A.S. Bharadwaj, 1991. A review of parameter sensitivity and adaptation in indirect vector controlled induction motor drive systems. *Power Electronics, IEEE Transactions on,* 6: 695-703.

Kuo-Kai, S. & S. Hsin-Jang, 1995. Variable structure current control for induction motor drives by space voltage vector PWM. *Industrial Electronics, IEEE Transactions on,* 42: 572-578.

Santisteban, J.A. & R.M. Stephan, 2001. Vector control methods for induction machines: an overview. *Education, IEEE Transactions on,* 44: 170-175.

Scottedward Hodel, A. & C.E. Hall, 2001. Variable-structure PID control to prevent integrator windup. *Industrial Electronics, IEEE Transactions on,* 48: 442-451.

Sousa, G.C.D., B.K. Bose, & J.G. Cleland, 1995. Fuzzy logic based on-line efficiency optimization control of an indirect vector-controlled induction motor drive. *Industrial Electronics, IEEE Transactions on,* 42: 192-198.

Vas. P., 1998. Sensorless vector and direct torque control, Oxford University Press.

Zelechowski, M., M.P. Kazmierkowski, & F. Blaabjerg, 2005. Year. Controller design for direct torque controlled space vector modulated (DTC-SVM) induction motor drives. *In:* Industrial Electronics, 2005. ISIE 2005. Proceedings of the IEEE International Symposium on, pp: 951-956.

[1]